An International Journal of Optimization and Control: Theories & Applications
ISSN: 2146-0957 eISSN: 2146-5703
Vol.16, No.5, pp.1883-1902 (2026)
https://doi.org/10.36922/IJOCTA026220097

RESEARCH ARTICLE

Thermal and mass transport analysis of solar-driven Williamson nanofluid flow over a stretching/shrinking wedge under an inclined magnetic field and heat generation

Amir Abbas[1,2]*, Akhlaqur Rahman[3], Maria Gulzar[1], Muhammad Farman[2,4,5], Mohamed Ahmed Hafez[6,7], Evren Hincal[2,8,9], Sk. Arefin. Shezan[10], and Naveed Ahmad[11]

[1]Department of Mathematics, Faculty of Natural Sciences and Technology, Baba Guru Nanak University, Nankana Sahib, Punjab, Pakistan

[2]Department of Mathematics, Mathematics Research Center, Near East University, Mersin 10, Turkey

[3]Department of Electrical Engineering and Industrial Automation, Engineering Institute of Technology, Melbourne, Victoria, Australia

[4]Department of Biostatistics and Medical Informatics, Faculty of Medicine, Karadeniz Technical University, Trabzon, Turkey

[5]International Center for Interdisciplinary Research in Sciences, The University of Lahore, Lahore, Punjab, Pakistan

[6]Faculty of Engineering and Quantity Surveying, INTI International University, Nilai, Negeri Sembilan, Malaysia

[7]Faculty of Management, Shinawatra University, Pathum Thani, Thailand

[8]Department of Mathematical Sciences, Saveetha School of Engineering, Saveetha Institute of Medical and Technical Sciences, Chennai, Tamil Nadu, India

[9]Research Center of Applied Mathematics, Khazar University, Baku, Azerbaijan

[10]Department of Electrical Engineering, Prince Faisal Centre for Renewable Energy Studies and Applications, Northern Border University, Arar, Northern Borders, Saudi Arabia

[11]Department of Chemical and Materials Engineering, College of Engineering, Northern Border University, Arar, Northern Borders, Saudi Arabia

amir.abbas@bgnu.edu.pk; akhlaqur.rahman@eit.edu.au; mariagulzar585@gmail.com; muhammad.farman@neu.edu.tr; mohdahmed.hafez@newinti.edu.my; evren.hincal@neu.edu.tr; shezan@nbu.edu.sa; naveed.ahmad@nbu.edu.sa

ARTICLE INFO

Article history:
Received: May 28, 2026
Revised: July 20, 2026
Accepted: July 20, 2026
Published online: August 21, 2026

Keywords:
Williamson fluid
Shrinking wedge
Stretching wedge
Solar radiation
Inclined magnetic field
Nanofluid

ABSTRACT

The growing energy consumption, increasing demand for efficient cooling systems, energy preservation in clean energy technology, cooling technology, and chemical engineering, and the applications of nanofluids and non-Newtonian fluids have attracted the attention of researchers and scientists in fluid mechanics. Because this demand cannot be accommodated in current systems using fluids of low thermal conductivity, fluids such as nanofluids with high thermal conductivity are used to improve cooling systems. Therefore, the combined study of the interactions among solar radiation, heat generation, and an inclined magnetic field in a two-phase Buongiorno nanofluid model coupled with a non-Newtonian Williamson fluid model, considering shrinking and stretching wedges along a flat plate and a full wedge, was conducted in the present study. The transformed differential equations were solved using MATLAB's bvp4c solver. The results show that increasing values of the Williamson fluid parameter, heat generation parameter, and inclined magnetic field parameter lead to a decrease in the velocity field for both the shrinking and stretching wedges along a flat plate and the full wedge under an inclined magnetic force $\gamma = \pi/6$. There is an increase in the temperature profile with increasing thermophoresis parameter and solar radiation parameter. The nanoparticle volume fraction increases with increasing values of

*Corresponding Author

the thermophoresis parameter for both cases of a wedge along a flat plate and a full wedge. A grid-independent test was performed to ensure that the solutions are grid-independent and that convergence of the solutions was maintained. The current results are compared with existing published results, which validates the accuracy of the present solutions.

1. Introduction

The flow of non-Newtonian fluids past stretching sheets has attracted the attention of researchers and scientists. The applications involve crystal formation, wire coating, pharmaceutical products, and food processing using the aforementioned fluid flow mechanism. This flow has several applications in manufacturing processes and aerospace engineering. The branch of non-Newtonian fluid mechanics plays a significant role in these fields. Ramesh *et al.*[1] investigated Williamson fluid flow past moving and stationary plates under slip and thermal boundary conditions. Priyadharshini *et al.*[2] proposed a study of Williamson fluid flow and heat transfer in a homogeneous porous medium. Asjad *et al.*[3] presented a two-phase nanofluid model to simulate Williamson fluid across an exponentially stretching sheet, incorporating bioconvection and thermal radiation effects. Rashid *et al.*[4] investigated the peristaltic flow of a Williamson fluid through a curved conduit under the influence of an applied magnetic field. Abbas *et al.*[5] performed a numerical study of the effect of magnetic forces on Williamson nanofluid flow along a nonlinear stretching sheet in a porous medium. They also incorporated viscous dissipation and heat generation effects in their study. Hussain[6] presented a study of hybrid nanofluid flow in a Williamson fluid with entropy generation analysis and thermal radiation effects. Several studies[7–10] have described non-Newtonian fluid flow processes with various flow properties and shaping conditions.

To increase the performance and compactness of electronic devices, heat transfer must be improved. Due to the low thermal conductivities of common cooling substances such as water and oil, heat transfer is not very effective. However, to improve thermal properties, substantially small particles (also known as nanoparticles) have been mixed with fluids to produce nanofluids. Such fluids have better thermal performance than conventional fluids. The nanofluid over a moving wedge with transpiration effects was investigated by Ishak *et al.*[11] Maaitah *et al.*[12] explored Williamson fluid flow along a horizontal plate fixed in a porous medium with viscous dissipation control. They included the Darcy–Forchheimer–Brinkman model in their conservation equations for the proposed process. Rashad *et al.*[13] investigated the magnetohydrodynamic (MHD) effects on Williamson hybrid nanofluid flow under Ohmic heating, convective boundary conditions, and thermal radiation.

Several studies have investigated Williamson fluid flow under different parametric conditions.[14-16] Salahuddin *et al.*[17] conducted a numerical simulation of heat transfer in Williamson fluid under the influence of magnetic forces, thermal diffusion, and diffusion-thermo effects, along with the effects of variable viscosity. Khan and Pop[18] explored heat and fluid flow in nanofluid across a sliding wedge. Mahendran *et al.*[19] investigated the effects of nanoparticles composed of titanium dioxide on the concentration of *Haematococcus pluvialis* biomass. Berrehal *et al.*[20] considered entropy generation in hybrid nanofluid flow along a moving wedge with convective boundary conditions. They used the single-phase model of nanofluid to study the mechanism of hybrid nanofluid flow. Sajid *et al.*[21] used a modified Buongiorno trihybrid nanofluid model coupled with a Prandtl–Eyring fluid model along a wedge to investigate the impact of endothermic/exothermic reactions and Cattaneo–Christov double diffusion, along with solar radiation and variable thermal conductivity, on heat and mass transfer. Mahanthesh *et al.*[22] explored hybrid nanofluid flow under the influence of a temperature-dependent heat source across an isothermal wedge. The effects of viscous dissipation and Joule heating were incorporated into the single-phase model of the nanofluid. Dawar *et al.*[23] performed an analysis of two-phase Williamson nanofluid flow past a cone and wedge with convective boundary conditions. They included the effects of non-isothermal and non-iso-solutal conditions. Nasir *et al.*[24] proposed an analysis of heat and mass transfer in Williamson nanofluid flow under stagnation-point conditions with nonlinear chemical reaction, liquid hydrogen diffusion, solar radiation, thermophoresis, and Brownian motion effects across a permeable wedge. Patil *et al.*[25] investigated Williamson nanofluid flow across a permeable stretching sheet under the influence of magnetic forces and thermal radiation, along with the effects of chemical reactions. Hussain *et al.*[26] conducted a study on radiative Williamson fluid flow along shrinking, static, and stretching wedges under solar radiation, convective boundary conditions, Ohmic heating, and suction/injection effects. Abbas *et al.*[27] conducted a theoretical analysis of MHD bioconvective Williamson nanofluid flow past an inclined moving sheet in a porous medium. Usman *et al.*[28] performed an analysis of Sutterby nanofluid flow across an elongating wedge in porous media. Comparable outcomes have been documented in prior works.[29,30]

Research on MHD non-Newtonian fluid flow across an extending sheet is important in engineering and industrial applications. During extrusion, a polymer sheet, for example, may be stretched under controlled conditions. The rate of cooling has a significant impact on the characteristics of the final product. Based on previous applications, a similar sheet can be drawn in a viscoelastic, electrically conducting fluid while subjected to a magnetic field, allowing the cooling rate to be controlled and the desired properties to be obtained. Sankari *et al.*[31] investigated MHD Williamson fluid flow along an exponentially stretching sheet in porous media. The effects of Joule heating, viscous dissipation, solar radiation, activation energy, and bioconvection involving gyrotactic microorganisms, along with Brownian motion and thermophoresis, were incorporated.

Obalalu *et al.*[32] conducted a study of three-dimensional Williamson fluid flow past an inclined stretching sheet, considering the effects of magnetic forces, chemical reactions, activation energy, thermal radiation, and heat sources and sinks. Sankari *et al.*[33] examined MHD Williamson bioconvective flow under the influence of non-uniform thermal conductivity, viscous dissipation, gyrotactic microorganisms, and activation energy. Priyadharshini *et al.*[34] explored MHD bioconvective phenomena in Williamson fluid flow across a stretching sheet using a machine-learning approach. Naz *et al.*[35] performed an analysis of MHD Williamson fluid flow over an exponentially stretching sheet, considering thermal radiation, Darcy medium effects, Ohmic heating, dissipation, Soret and Dufour effects, along with entropy generation. Swalmeh *et al.*[36] examined Williamson ferrofluid flow past a stretching sheet under the influence of magnetic forces and thermal radiation. Zafar *et al.*[37] theoretically studied the bioconvection of Williamson nanofluid flow considering MHD nanofluid flow over a stretching sheet under the influence of gyrotactic microorganisms and nanoparticle fraction effects. Akbar *et al.*[38] investigated three-dimensional magneto-Williamson fluid flow over a linearly expanding sheet. The effects of heat source, bioconvection, Joule heating, Brownian motion, and thermophoresis diffusion were included in their study. Znaidia *et al.*[39] investigated mixed-convective magneto-Williamson fluid flow coupled with a Darcy–Brinkman permeable medium and the Brinkman–Maxwell–Garnett model in a vertical cylinder. Zafar *et al.*[40] investigated Williamson fluid flow over a stretching lubricant surface, considering the effects of magnetic forces, activation energy, and partial slipping.

The increasing growth of modern technology to meet the current global energy demand has created a need for efficient heat-transfer systems. Many heat-transfer mechanisms involve wedge geometry; hence, they can be enhanced using highly efficient nanofluids for improved thermal management. There are many practical applications of the Williamson fluid model, which exhibits shear-thinning behavior and is therefore more realistic than many other classical non-Newtonian fluid models. Understanding and predicting the flow and thermal transport processes of such fluids are therefore highly significant. Solar radiation is a significant factor in sustainable and renewable energy technologies. The magnetic field is highly relevant to cooling systems because they may involve electrically conducting fluids; hence, the inclusion of MHD effects is important. In addition, internal heat generation or absorption plays a vital role in processes involving chemical reactions, nuclear systems, and energy conversion devices, further influencing the thermal field. Shrinking and stretching wedges are important in polymer extrusion, aerodynamic flows, and coating processes. The interaction of all these parameters within a combined framework plays a vital role in thermal management systems. Therefore, the motivation for the current study is to develop a realistic and comprehensive model that captures the combined effects of Williamson non-Newtonian nanofluid flow, thermal radiation, internal heat generation, and an inclined magnetic field on shrinking and stretching wedges for both flat-plate and full-wedge configurations. The outcomes of this work are expected to provide valuable insights for the design and optimization of advanced thermal systems in renewable energy, industrial processing, and MHD-based technologies. The comparative literature relevant to the development of the current model is presented in **Table 1**.

2. Problem formulation

Consider a two-dimensional, incompressible, steady, viscous, Williamson nanofluid flow over a stretching and shrinking wedge. The effects of an inclined Lorentz force and solar radiation are assumed in the flow equations. The effects of heat generation are also considered in the present problem. The vertical and horizontal components of velocity are u and v, respectively. The temperature of the surface is T_w, and the nanoparticle volume fraction at the surface is C_w. T_∞ and C_∞ are the temperature and nanoparticle volume fraction in the free stream region, respectively. The wedge is considered under both shrinking and stretching conditions. The flow is induced due to the stretching and compressed due to the shrinking of the wedge. The flow configuration is shown in **Figure 1**. Following previous studies[1,18,23-28], the model equations are as follows:

$$\frac{\partial u}{\partial x}+\frac{\partial v}{\partial y}=0 \tag{1}$$

$$\begin{aligned} u\frac{\partial u}{\partial x}+v\frac{\partial u}{\partial y}&=u_e\frac{du_e}{dx}+\upsilon\frac{\partial^2 u}{\partial y^2}+\sqrt{2}\mu\Gamma\frac{\partial u}{\partial y}\frac{\partial^2 u}{\partial y^2}\\ &-\frac{\sigma B_o^2}{\rho}\left(u-u_e\right)\sin\left(\gamma\right)^2+g\beta_T\left(T-T_\infty\right)+g\beta_C\left(C-C_\infty\right)\end{aligned} \tag{2}$$

$$\begin{aligned} u\frac{\partial T}{\partial x}+v\frac{\partial T}{\partial y}&=\frac{k}{\left(\rho C_p\right)_f}\frac{\partial^2 T}{\partial y^2}-\frac{1}{\left(\rho C_p\right)_f}\frac{\partial q_r}{\partial y}\\ &+\tau\left\{D_B\frac{\partial C}{\partial y}\frac{\partial T}{\partial y}+\frac{DT}{T_\infty}\left(\frac{\partial T}{\partial y}\right)^2\right\}+\frac{Q_O\left(T-T_w\right)}{\left(\rho C_p\right)_f}\end{aligned} \tag{3}$$

$$u\frac{\partial C}{\partial x}+v\frac{\partial C}{\partial y}=D_B\frac{\partial^2 C}{\partial y^2}+\frac{D_T}{T_\infty}\frac{\partial^2 T}{\partial y^2} \tag{4}$$

Depending on the boundary conditions,

$$\begin{aligned} &u=u_w\left(x\right)=-\lambda u_e\left(x\right),\ v=0,\\ &T=T_w,\ C=C_w,\ at\ y=0\\ &u\to u_e\left(x\right),\ T\to T_\infty, C\to C_\infty \quad as\ y\to\infty\end{aligned} \tag{5}$$

Table 1. Literature review highlighting the novelty and development of the present study

Study	Williamson fluid	Buongiorno nanofluid	Stretching/ shrinking wedge	Inclined magnetic field	Thermal radiation	Heat generation
Ramesh *et al.*[1]	Yes	No	No	No	No	No
Khan and Pop[18]	No	Yes	Yes	No	No	No
Dawar *et al.*[23]	Yes	Yes	Yes	No	No	No
Nasir *et al.*[24]	Yes	Yes	Yes	No	No	No
Patil *et al.*[25]	Yes	Yes	No	No	Yes	No
Hussain *et al.*[26]	Yes	No	Yes	No	Yes	No
Abbas *et al.*[27]	Yes	Yes	No	No	No	No
Usman *et al.*[28]	No	Yes	Yes	No	No	No
The present study	Yes	Yes	Yes	Yes	Yes	Yes

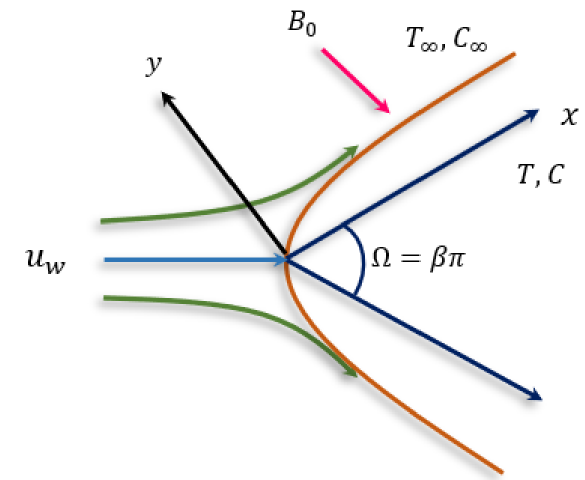

Figure 1. Flow structure

For the similarity solutions, it is assumed that $u_w\left(x\right)=ax^m, u_e\left(x\right)=cx^m$, where $a, c, and\ m, with\ 0\le m\le 1$, are constants. A moving constant parameter $\lambda=c/a$ coressponds to a stretching wedge when $\lambda<0$, a shrinking wedge when $\lambda>0$, and a fixed wedge when $\lambda=0$. The pressure gradient along the wedge is given by $\frac{du_e}{dx}=\frac{mu_e}{x}$, where m is the wedge parameter.

The radiative heat flux in the y-direction is given using the Rosseland approximation as follows:

$$q_r=\frac{4\sigma^*}{3K_R}\frac{\partial T^4}{\partial y}. \tag{6}$$

Here, K_R is termed the mean absorption coefficient, and σ^* is called the Stefan–Boltzmann constant. A linear approximation of T^4 is defined using a Taylor series expansion about T_∞ is as:

$$\mathrm{T}^4\approx 4\mathrm{T}_\infty^3\mathrm{T}-3\mathrm{T}_\infty^4 \tag{7}$$

where T_∞ is the ambient temperature of the fluid.

Now, **Equation 7** becomes

$$q_r=-\frac{4\sigma^*\mathrm{T}_\infty^3}{3K_R}\frac{\partial T}{\partial y} \tag{8}$$

The mathematical symbols included in **Equations 1–8** are defined in **Table 2**.

3. Solution methodology

This section elaborates on the solution methodology of the current model in detail.

3.1. Similarity variable formulation

The direct simulation of the nonlinear partial differential equations is complex; therefore, these equations are transformed into ordinary differential equations using suitable similarity transformation variables (**Equation 9**).[18]

$$\begin{aligned} &\psi=\left(\frac{2u_e x\nu}{1+m}\right)f\left(\eta\right),\eta=\left(\frac{\left(1+m\right)u_e}{2x\nu}\right)^{\frac{1}{2}}y,\\ &\theta\left(\eta\right)=\frac{\left(T-T_\infty\right)}{\left(T_w-T_\infty\right)},\phi\left(\eta\right)=\frac{\left(C-C_\infty\right)}{\left(C_w-C_\infty\right)}\end{aligned} \tag{9}$$

The transformed boundary layer equations obtained using the stream function formulation in **Equation 9** are as follows:

$$\begin{aligned} &f'''+Wf'''f''+ff''+\beta(1-f'^2)\\ &+M(f'-1)\sin\left(\gamma\right)^2+\theta\lambda_{T2T}+\phi\lambda_{C2T}=0\end{aligned} \tag{10}$$

$$\frac{1}{Pr}\left(1+\frac{4}{3}Rd\right)\theta''+f\theta'+Nt\theta'^2+Nb\theta'\phi'+Q\theta=0 \tag{11}$$

$$\frac{1}{Sc}\phi''+f\phi'+\frac{Nt}{Nb}\theta''=0 \tag{12}$$

Table 2. Physical symbols along with their definitions

Physical symbol	Definition	Physical symbol	Definition
m	Wedge parameter	σ	Electrical conductivity
Γ	Williamson fluid time constant	ρ	Fluid density
u_e	External velocity scale	γ	Angle of magnetic field with respect to the surface
ν	Kinematic viscosity	g	Gravitational acceleration
x	Distance along wedge	β_C	Solutal expansion coefficients
m	Wedge parameter	$(T_w - T_\infty), (C - C_\infty)$	Wall–ambient difference
$m = 0, m = 1$	Flat plate, wedge	T	Fluid temperature
B_o	Magnetic field	C	Mass concentration
β_T	Thermal expansion coefficients	C_w	Mass concentration at surface
T_w	Fluid temperature at surface	T_∞	Fluid temperature at infinity
C_∞	Mass concentration at infinity	k	Thermal conductivity
K_R	Mean absorption coefficient	σ^*	Stefan–Boltzmann constant
α	Thermal diffusivity	D_B	Brownian diffusion coefficient
$(\rho c)_p$	Nanoparticle heat capacity	$(\rho c)_f$	Fluid heat capacity
D_T	Thermophoretic diffusion coefficient	Q_o	Volumetric heat generation
a, c	Constants are positive constants	$\tau = \dfrac{(\rho c)_p}{(\rho c)_f}$	Heat capacity ratio parameter
u, v	Velocity components	x, y	Horizontal and vertical coordinates

Flow conditions:

$$f = 0, f' = -\lambda, \theta = 1, \phi = 1 \; as\, \eta \to 0$$
$$f' = 1, \theta = 0, \phi = 0 \; as\, \eta \to \infty \tag{13}$$

The parameters appearing in **Equations 10–13** are given in **Table 3**.

3.2. Solution technique

The transformed model in the form of ordinary differential **Equations 10–12**, with boundary conditions given in **Equation 13**, is first reduced to a set of first-order differential equations and then solved using the MATLAB bvp4c solver. The bvp4c solver is based on a collocation technique using a three-stage Lobatto formula. In the numerical simulation, a maximum value of $\eta = 10.0$ is taken. This solver solves the set of algebraic equations obtained from the boundary conditions and collocation conditions applied to all the subintervals. The procedure to reduce the equations to first-order differential equations is given below:

$$P_1 = f, P_2 = f', P_3 = f'', P_4 = \theta,$$
$$P_5 = \theta', P_6 = \phi, P_7 = \phi' \tag{14}$$

$$\mathrm{PP1} = -\frac{\begin{pmatrix} \left(P_1 * \mathrm{P}_3 + \beta * (1 - P_2^{\,2})\right) + \left(M * P_2 - 1\right) * \sin(\gamma)^2 \\ + P_4 * \lambda_{T2T} + P_6 * \lambda_{C2T}) \end{pmatrix}}{\left(1 + We * P_3\right)} \tag{15}$$

$$PP2 = -\mathrm{Pr} * \frac{\left(P_1 * P_5 + Nt * P_5^{\,2} + Nb * P_5 * P_7 - Q * P_4\right)}{\left(1 + \frac{4}{3} Rd\right)} \tag{16}$$

$$PP3 = Sc * \left(P_1 * P_7 + \frac{Nt}{Nb} * PP2 \right) \tag{17}$$

Boundary conditions:

$$\mathrm{P}_1 = 0, \mathrm{P}_2 = -\lambda, \mathrm{P}_4 = 1, \mathrm{P}_6 = 1 \;\text{ at }\; \eta = 0,$$
$$\mathrm{P}_2 = 1, \mathrm{P}_4 = 0, \mathrm{P}_6 = 0 \;\text{as}\; \eta \to \infty \tag{18}$$

This system is put into algorithm of bvpc4 in MATLAB for the final solutions. The numerical solutions of the physical variables are determined in graphical and tabular form and have been discussed in the next section.

4. Grid-independent test and code validation

The current section is devoted to observing and presenting the stability of the solutions obtained using the numerical scheme through a grid-independent test and a comparison between the present and published results.

4.1. Grid-independent test

The independence of the solutions from the number of grid points or mesh size (mesh refinement) is essential to ensure that the solutions are not affected by the number of grid points or discretization size. This test demonstrates whether the numerical solutions are sufficiently independent of the computational grid. In this study, grid refinement was conducted by increasing the number of grid points from 50 to 600. The values of $-\theta$ for increasing numbers of grid points are determined when other parameters are fixed at their values, as presented in **Table 4**. There is comparatively large difference between the values of $-\theta$ at 50 and 100 grid points, but this variation decreases thereafter, and the values eventually remain nearly constant, indicating that the solutions are independent of the number of grid points. The solutions become convergent when the number of grid points increases from 400 to 600. The reported numerical solutions in the current study are considered independent of the discretization because of the negligible changes observed with grid refinement, which confirms the numerical stability and reliability of the employed numerical technique.

4.2. Code validation via comparison of results

For the validation of the current solutions obtained using the BVP4C code implemented in MATLAB, the results were compared with previously published results for the skin-friction coefficient. This comparison was made under special cases by assigning specific values to the relevant parameters. The comparison shows excellent agreement between the present and previously published results, demonstrating the accuracy and reliability of the current numerical results. This agreement supports the validity and accuracy of the numerical scheme applied to the proposed model. Hence, the numerical solutions and the computational scheme were validated.

Additionally, the current solutions for the rate of heat transfer, $-\theta'(0)$, obtained for different values of m, were compared with previously published results. The current and previously published values of $-\theta'(0)$ are presented in **Tables 5** and **6**, and demonstrate a good degree of agreement. This agreement further supports the validity of the current numerical solutions.

Table 3. Definition of the pertinent parameters appearing in Equations 10–13

Parameter name	Definition	Parameter name	Definition
Solutal buoyancy parameter	$\lambda_{C2T} = \dfrac{g\beta_T (C_w - C_\infty) x}{u_e^2}$	Williamson fluid parameter	$W = \Gamma \sqrt{\dfrac{2u_e^3}{(1+m)\nu x}}$
Prandtl number	$Pr = \dfrac{\upsilon}{\alpha}$	Thermal buoyancy parameter	$\lambda_{T2T} = \dfrac{g\beta_T (T_w - T_\infty) x}{u_e^2}$
Schmidt number	$Sc = \dfrac{\upsilon}{D_B}$	Magnetic field parameter	$M = \dfrac{\sigma B_o^2}{\rho u_e} \sqrt{\dfrac{2\nu x}{(1+m) u_e}}$
Thermophoresis parameter	$Nt = \dfrac{(\rho c)_p D_T \Delta T}{(\rho c)_f T_\infty \nu}$	Solar radiation parameter	$Rd = \dfrac{4\sigma^* T_\infty^3}{k K_R}$
Angle of inclination of the magnetic field	γ	Brownian motion parameter	$Nb = \dfrac{(\rho c)_p D_B (\phi_w - \phi_\infty)}{(\rho c)_f \nu}$
measure of the pressure gradient effect	$\beta = \dfrac{2m}{1+m}$	Heat generation parameter	$Q = \dfrac{Q_o}{\rho C_p (T_w - T_\infty) u_e} \sqrt{\dfrac{2\nu x}{(1+m) u_e}}$

Table 4. Grid independence test for Williamson nanofluid flow

Number of grid points	$-\theta'(0)$
50	1.5032
100	1.5051
200	1.5061
400	1.5065
500	1.5065
600	1.5065

Parameters:
$\lambda_T = 0.1; \lambda_C = 0.1; \lambda = -0.1; m = 0.0; Pr = 7.0;$
$Sc = 3.1; W = 7.1; Rd = 10.1; Nt = 0.1; Nb = 0.1;$
$M = 10.0; Q = 6.1; at\, \gamma = \pi / 30.$

5. Results and discussion

This section is devoted to discussing the physical effects of the pertinent parameters on the physical quantities, such as the velocity profile $f'(\eta)$, temperature profile $\theta(\eta)$, and mass concentration $\phi(\eta)$, as well as their derivatives—skin friction $f''(\eta)$, heat transfer rate $\theta'(\eta)$, and mass transfer rate $\phi'(\eta)$. Numerical results are presented in both graphical and tabulated form for the shrinking wedge and stretching wedge, with consideration of the flat plate and wedge geometries.

In this study, the parametric effects of the buoyancy parameter λ_T, modified buoyancy parameter λ_C, heat generation parameter Q, inclined magnetic field parameter M, thermophoresis parameter Nt, Prandtl number Pr, Brownian motion parameter Nb, solar radiation parameter Rd, Schmidt number Sc, angle of magnetic field with respect to the surface γ, wedge parameter m, shrinking wedge and stretching wedge parameter λ, and Williamson fluid parameter W on the physical quantities of interest are considered.

The ranges of the parameters for the current study were:

$$0 \le \lambda_T \le 0.1, 0 \le \lambda_C \le 0.1, 0 \le Q \le 6.1, 0 \le M \le 10, -0.1 \le \lambda \le 0.1,$$
$$0 \le m \le 1, 0 \le W \le 7.1, 0 \le Rd \le 10.1, 0 \le Nt \le 7.1, 0 \le Nb \le 10.0,$$
$$0 \le Sc \le 1.1, 0 \le \gamma \le \frac{\pi}{6}, 0 \le Pr \le 7.0.$$

Table 5. Numerical comparison of $f''(0)$ for Williamson nanofluid flow

m	$f''(0)$	
	Previous study (Khan and Pop[18])	Present study
0.0	0.4696	0.4493
0.09	0.6550	0.6535
0.2	0.8021	0.8021
0.33	0.9277	0.9250
0.5	1.0389	1.0389
1.0	1.2326	1.2326

Parameters:
$\lambda_T = 0.0; \lambda_C = 0.0; \lambda = 0.0;; Pr = 1.0; Sc = 0.1; W = 0.0;$
$Rd = 0.0; Nt = 0.1; Nb = 0.1; M = 0.0; Q = 0.0; at\, \gamma = 0.0.$

Table 6. Comparison of numerical values of heat transfer rate $-\theta'(0)$ for distinct values of m

Parameter (m)	$-\theta'(0)$	
	Present study	Previous study (Khan and Pop[18])
0.0	0.8768	0.8769
1.0	1.1267	1.1279

The chosen ranges of each parameter are justified in relation to realistic engineering systems as follows:

(i) The selected range of the thermal buoyancy parameter represents mixed convection, in which forced convection is more prominent than natural convection, but buoyancy effects remain substantial. Such conditions are encountered in solar collectors, vertical heat exchangers, and cooling channels.

(ii) The selected range of the modified (solutal) buoyancy parameter represents weak concentration-driven buoyancy effects, typically occurring in chemical reactors, membrane separation processes, drying technologies, and mass-transfer equipment.

(iii) The selected range of volumetric heat generation corresponds to conditions in nuclear reactors, chemical reactors, electronic devices, battery thermal management systems, and exothermic industrial processes, where internal heat sources substantially affect system behavior.

(iv) The selected range of the inclined magnetic field parameter represents weak to moderately strong magnetic fields, commonly found in electromagnetic flow control, metallurgical processing, liquid-metal heat exchangers, and MHD cooling systems, where Lorentz forces substantially influence the flow system.

(v) The selected small positive and negative values of the shrinking and stretching parameter are aligned with engineering systems such as polymer extrusion, glass-fiber production, wire drawing, continuous casting, and coating processes, ensuring stable boundary-layer solutions.

(vi) The chosen values of the wedge parameter, with $m = 0$ for a flat plate and $m = 1$ for a wedge, represent aerodynamic wedges, turbine blades, and tapered engineering components.

(vii) The chosen values of W indicate weak to moderately strong non-Newtonian (shear-thinning) influences in Williamson fluids, as seen in polymer processing, lubricants, paints, biological fluids, food processing, and coating technologies. When larger values of W are considered, robust elastic and shear-thinning behavior is observed, ensuring that the selected values are appropriate for the analysis of practical non-Newtonian transport processes while maintaining physically realistic boundary-layer flow conditions.

(viii) The chosen range of values for the radiation parameter corresponds to conditions found in solar thermal collectors, thermal insulation applications, concentrated solar power systems, and high-temperature furnaces, where radiative heat transfer becomes comparable to conduction.

(ix) The range of values for the thermophoresis parameter is physically aligned with applications in solar energy devices, aerosol transport, nanoparticle deposition processes, and combustion systems, where nanoparticle migration due to thermophoresis is highly significant.

(x) The selected values of the Brownian motion parameter represent nanofluids containing nanoparticles of varying concentrations and sizes, utilized in solar collectors, electronic cooling systems, automotive radiators, and heat exchangers, in which thermal transport is enhanced by Brownian diffusion.

(xi) The selected value of inclination angles up to 30° simulates practical situations where magnetic fields cannot always be applied normal to the surface, such as in electromagnetic manufacturing, crystal growth, and MHD flow control devices.

(xii) For the selected range of the Prandtl number, the analysis can be applied to a wide range of engineering cooling and heating systems, since the spectrum includes fluids ranging from water ($\Pr \approx 7$) to liquid metals (low Pr).

(xiii) The range of Schmidt number corresponds to gases and diluted liquid mixtures, encountered in chemical engineering applications, drying procedures, mass-transfer equipment, and pollution dispersion studies.

Figure 2 presents the impact of the Williamson fluid parameter W on f' for both shrinking ($\lambda = 0.1, \lambda > 0$) and stretching wedge ($\lambda = -0.1, \lambda < 0$), along the flat plate and wedge. The findings demonstrate that as W increases, the velocity profile declines for both shrinking and stretching wedges along the flat plate ($m = 0.0$) and wedge ($m = 1.0$). It is noteworthy that the difference between the curves for the flat plate and wedge is smaller in the stretching wedge than in the shrinking wedge. The physical reasoning behind this is that for higher values of W, more non-Newtonian effects appear. At lower shear rates, larger viscosity reduction is observed; however, the apparent resistance to flow increases within the boundary layer, leading to a reduction in the velocity field. In the shrinking wedge, non-Newtonian effects are more prominent, and the free stream decelerates, resulting in a larger difference between the flat plate and wedge, and vice versa.

Figure 3 presents the behavior of velocity profiles against increasing values of the heat generation Q for shrinking and stretching wedges, considering both the flat plate ($m = 0.0$) and wedge ($m = 1.0$). It has been observed that as Q increases, the velocity profile increases in both cases—shrinking and stretching wedges—for both flat plate and wedge geometries.

Figure 4 depicts the impact of the inclined Lorentz force associated with the magnetic field parameter M on f' for both shrinking and stretching wedges, with graphs plotted for the flat plate and wedge. The physics of M indicates that as it increases, the corresponding inclined Lorentz force also increases, generating resistance that leads to a reduction in f'.

Figure 5 presents the influence of the heat generation parameter Q on temperature profiles θ in both shrinking ($\lambda = 0.1, \lambda > 0$) and stretching wedge ($\lambda = -0.1, \lambda < 0$), corresponding to the domains of the flat plate and wedge. With the increase in internal heat generation, the fluid temperature increases accordingly.

Figure 6 depicts the physical influence of the radiation parameter Rd on θ for shrinking and stretching wedges. The graphs illustrate that as Rd increases, the temperature profile also increases in both flat plate and wedge cases. It is noteworthy that in the shrinking wedge, the difference between θ curves is larger than in the stretching wedge. The basic purpose of including Rd in the energy equation is to enhance the fluid temperature through radiative heat transfer, which is effectively achieved.

Figure 7 shows the impact of the thermophoresis parameter Nt on θ for both shrinking ($\lambda = 0.1, \lambda > 0$) and stretching wedge ($\lambda = -0.1$, $\lambda < 0$). The plots demonstrate that increasing Nt leads to an enhancement in θ. It is a well-established fact that the thermophoresis parameter represents the migration of nanoparticles from hot regions to cold regions due to temperature gradients. The migration of nanoparticles from the heated surface into the fluid carries extra energy, thereby increasing thermal energy distribution and raising θ. It is observed that the difference between temperature profile curves is larger in the shrinking wedge compared to the stretching wedge. This occurs because compression in the fluid near the surface leads to greater nanoparticle accumulation, resulting in higher temperatures.

Figure 8 shows the influence of the Brownian motion parameter Nb on θ for both shrinking ($\lambda = 0.1$, $\lambda > 0$) and stretching wedges ($\lambda = -0.1$, $\lambda < 0$). The plots demonstrate that increasing Nb leads to an enhancement in θ. The parameter Nb represents the random motion of nanoparticles due to molecular collisions; this mixing motion enhances the temperature profile. This random motion also causes attenuation of the temperature gradient near the wall, particularly in the shrinking wedge. In the stretching wedge, Brownian motion is less effective compared to the shrinking wedge.

Figure 9 presents the effects of the thermophoresis parameter Nt on the nanoparticle volume fraction (concentration) ϕ for shrinking and stretching wedges along the flat plate and full wedge. The graphs show an increasing trend with rising values of Nt for both geometries. Physically, this is consistent: as Nt increases, nanoparticles are pushed away from the heated surface but do not immediately disperse into the bulk fluid. Instead, they accumulate near the surface, which explains the increase in nanoparticle volume concentration across all cases.

Figure 10 depicts the parametric effect of the Brownian motion parameter Nb on nanoparticle volume fraction (concentration) for shrinking and stretching wedges along the flat plate ($m = 0.0$) and wedge ($m = 1.0$). The graphical solutions show that ϕ exhibits a decreasing trend with increasing magnitudes of Nb. It is noteworthy that the difference between the curves for the shrinking wedge, as well as between the flat plate and wedge, is comparatively larger than in the stretching wedge. The impact of Nb arises because nanoparticles move randomly from regions of higher concentration to lower concentration, causing greater diffusion and mixing, which reduces concentration in the boundary layer. In the shrinking wedge, Brownian motion effects are stronger due to fluid compression, whereas in the stretching wedge they are weaker. Furthermore, in the flat plate case, no pressure gradient exists, leading to higher values compared to the wedge case, where a significant pressure gradient is present. All of the graphs satisfy the boundary conditions asymptotically.

Table 7 presents the impact of the inclined magnetic field parameter on skin friction $f''(0)$, rate of heat transfer $\theta'(0)$, and rate of nanoparticle volume fraction $\phi'(0)$ for the streetching wedge. As M represents the resistive force, the fluid undergoes compression in the wedge, so the velocity gradient increases at the wall, leading to an increase in skin friction. In the wedge, the pressure gradient, along with the Lorentz force, enhances shear formation. The resistive force reduces the convective transport; hence, thermal energy accumulates, resulting in a reduction in the heat transfer rate.

As fluid motion is suppressed with increasing M, Brownian motion and thermophoresis dominate. Therefore, a steeper concentration gradient is observed, leading to an increase in the nanoparticle mass transfer rate. It is noteworthy that for the flat plate, values are greater than those in the wedge because in the wedge there is a pressure gradient, whereas in the flat plate there is none. Hence, the heat transfer rate is higher in the flat plate than in the wedge.

For the stretching wedge:

(i) Flat plate: $f''(0)$ increases by 68.79%, $\theta'(0)$ increases by 7.36%, and $\phi'(0)$ increases by 76.08%.

(ii) Wedge: $f''(0)$ increases by 38.17%, $\theta'(0)$ increases by 4.36%, and $\phi'(0)$ increases by 29.45%.

Table 8 shows the same properties as those presented in **Table 7** for the same parametric situation, but for the shrinking wedge. It has been noted that in the shrinking wedge, skin friction is 0.8990 for $M = 3.0$, 1.2897 for $M = 7.0$, and 1.5174 for $M = 10.0$. On the other hand, for the stretching wedge, skin friction is 0.5800 for $M = 3.0$, 0.8226 for $M = 7.0$, and 0.9646 for $M = 10.0$ along the flat plate ($m = 0.0$).

It has also been noted that in the shrinking wedge, the heat transfer values are 0.7365 for $M = 3.0$, 0.6980 for $M = 7.0$, and 0.6823 for $M = 10.0$. Conversely, for the stretching wedge, the heat transfer rate is 0.6911 for $M = 3.0$, 0.6648 for $M = 7.0$, and 0.6534 for $M = 10.0$ along the flat plate ($m = 0.0$).

For the shrinking wedge, the nanoparticle volume concentration rate starts at 0.1551 for $M = 3.0$, 0.2376 for $M = 7.0$, and 0.2731 for $M = 10.0$. On the other hand, for the stretching wedge, the nanoparticle volume concentration rate is 0.2570 for $M = 3.0$, 0.3174 for $M = 7.0$, and 0.3445 for $M = 10.0$ along the flat plate ($m = 0.0$).

The same pattern in all qualities is observed for the wedge ($m = 1.0$), but with different numerical values. The nanoparticles mass transfer rate in the stretching wedge is greater than that in the shrinking wedge. This occurs because in the shrinking wedge, the fluid is compressed and accelerated, whereas in the stretching wedge, the fluid experiences less compression.

For the flat plate in the stretching wedge: $f''(0)$ increases by 66.31%, $\theta'(0)$ increases by 5.46%, and $\phi'(0)$ increases by 34.05%. For the wedge case, $f''(0)$ increases by 37.36%, $\theta'(0)$ increases by 3.34%, and $\phi'(0)$ increases by 16.92%.

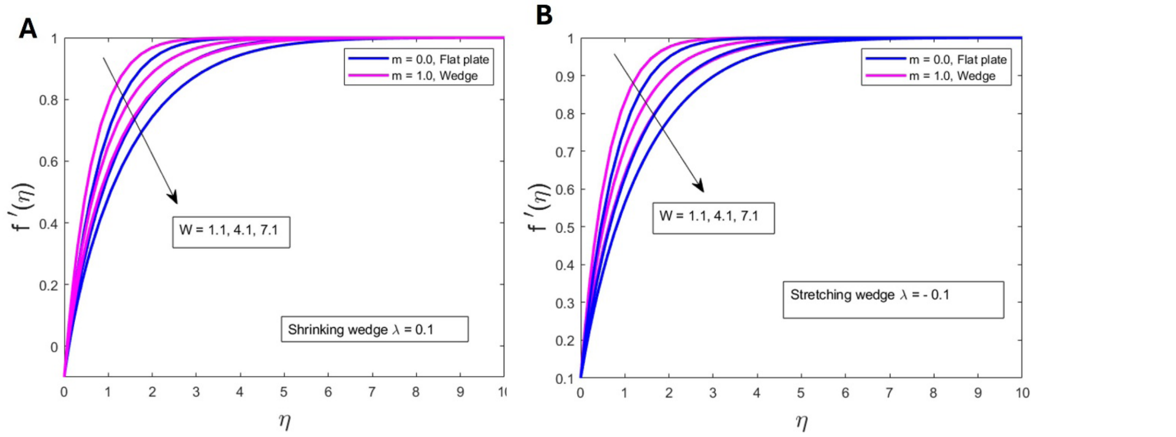

Figure 2. Velocity profiles f' for different values of W on (A) shrinking wedge and (B) stretching wedge. Parameters: $\lambda_T = 0.1; \lambda_C = 0.1; Pr = 7.0; Sc = 1.1; Rd = 10.1; Nt = 0.1; Nb = 10.0; \gamma = \frac{\pi}{6}; Q = 6.1; M = 5.0.$

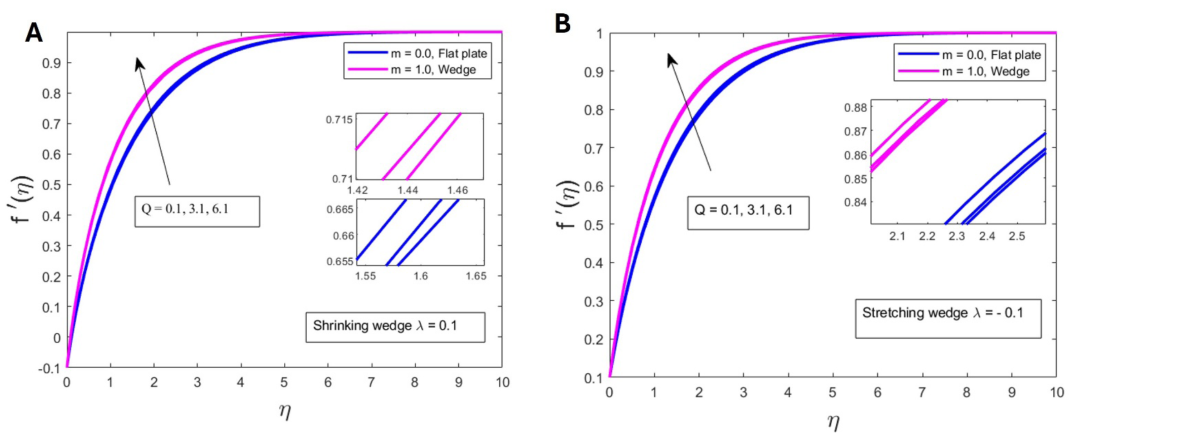

Figure 3. Velocity profiles f' for different values of Q on (A) shrinking wedge and (B) stretching. Parameters: $\lambda_T = 0.1; \lambda_C = 0.1; Pr = 7.0; Sc = 1.1; W = 7.1; Rd = 10.1; Nt = 0.1; Nb = 10.0; \gamma = \frac{\pi}{6}; M = 5.0.$

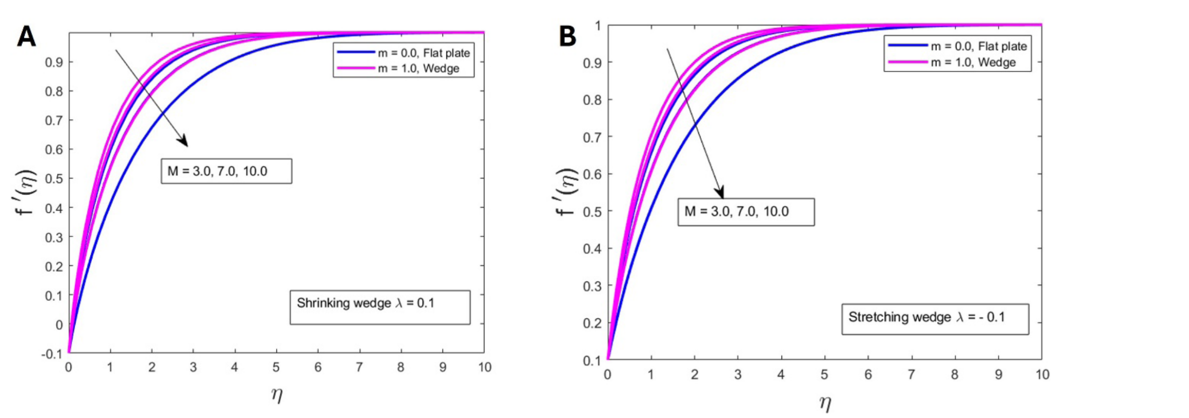

Figure 4. Velocity profiles f' for different values of M on (A) shrinking wedge and (B) stretching wedge. Parameters: $\lambda_T = 0.1; \lambda_C = 0.1; Pr = 7.0; Sc = 1.1; W = 7.1; Rd = 10.1; Nt = 0.1; Q = 6.1, Nb = 10.0; \gamma = \frac{\pi}{6}; Nt = 7.1.$

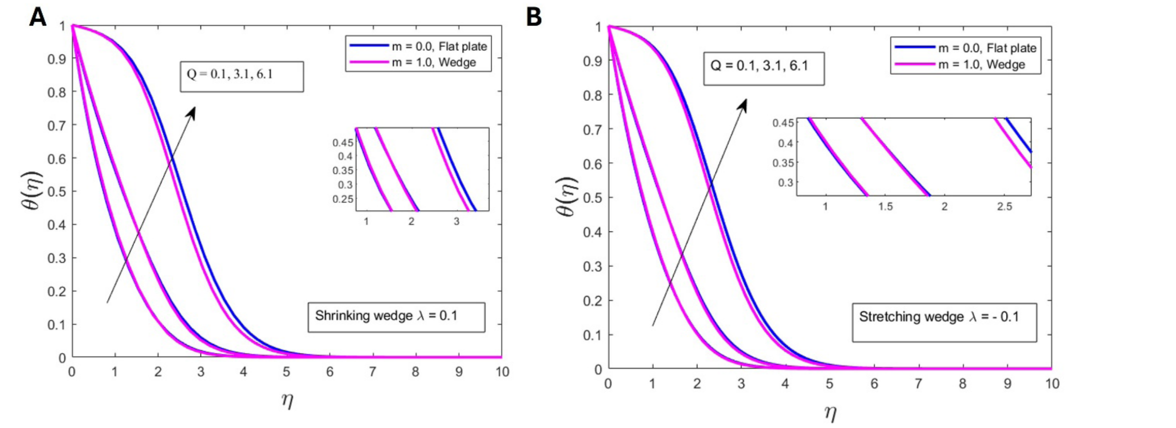

Figure 5. Temperature profiles θ for different values of Q on (A) shrinking wedge and (B) stretching wedge. Parameters: $\lambda_T = 0.1; \lambda_C = 0.1; Pr = 7.0; Sc = 1.1; W = 7.1; Rd = 10.1; Nt = 0.1; Nb = 10.0; \gamma = \frac{\pi}{6}; M = 5.0.$

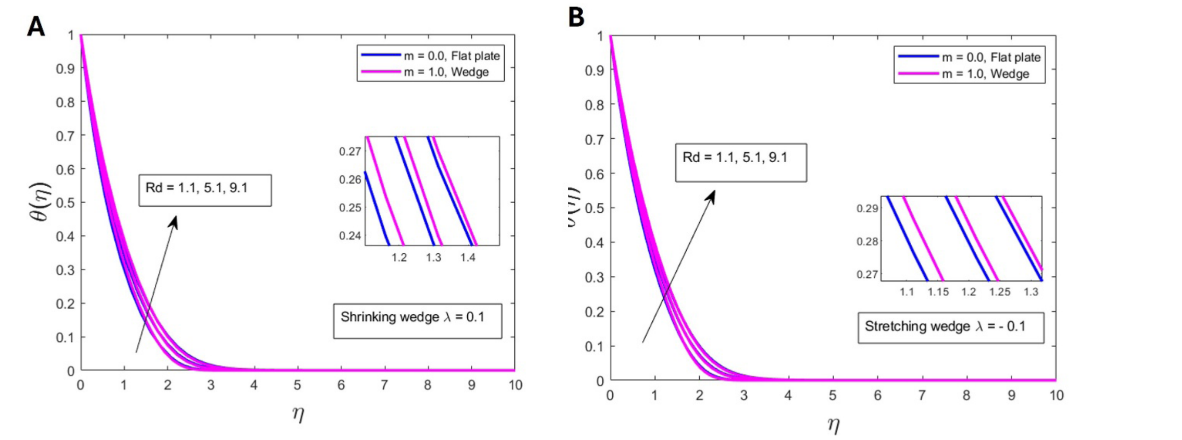

Figure 6. Temperature profiles θ for different values of Rd on (A) shrinking wedge and (B) stretching wedge. Parameters: $\lambda_T = 0.1; \lambda_C = 0.1; Pr = 7.0; Sc = 1.1; W = 7.1; Q = 6.1; Nt = 0.1; Nb = 10.0; \gamma = \frac{\pi}{6}; M = 5.0.$

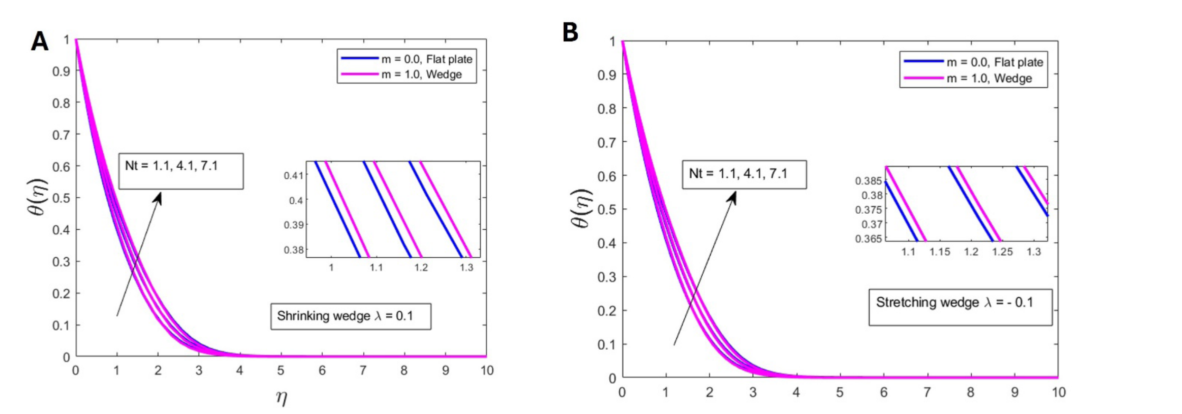

Figure 7. Temperature profiles θ for different values of Nt on (A) shrinking wedge and (B) stretching wedge. Parameters: $\lambda_T = 0.1; \lambda_C = 0.1; Pr = 7.0; Sc = 1.1; W = 7.1; Q = 6.1; Rd = 10.1; Nb = 10.0; \gamma = \frac{\pi}{6}; M = 5.0.$

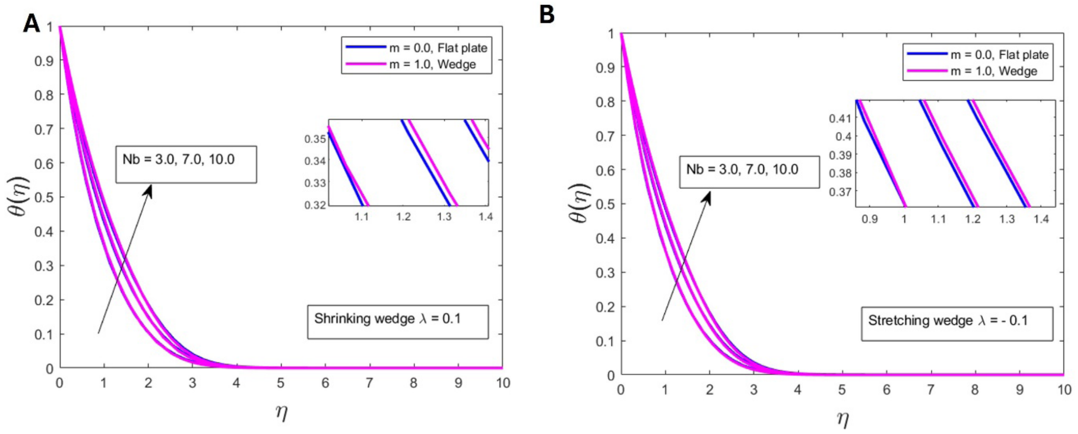

Figure 8. Temperature profiles θ for different values of Nb on (A) shrinking wedge and (B) stretching wedge. Parameters: $\lambda_T = 0.1; \lambda_C = 0.1; Pr = 7.0; Sc = 1.1; W = 7.1; Q = 6.1; Rd = 10.1; Nt = 7.1; \gamma = \dfrac{\pi}{6}; M = 5.0.$

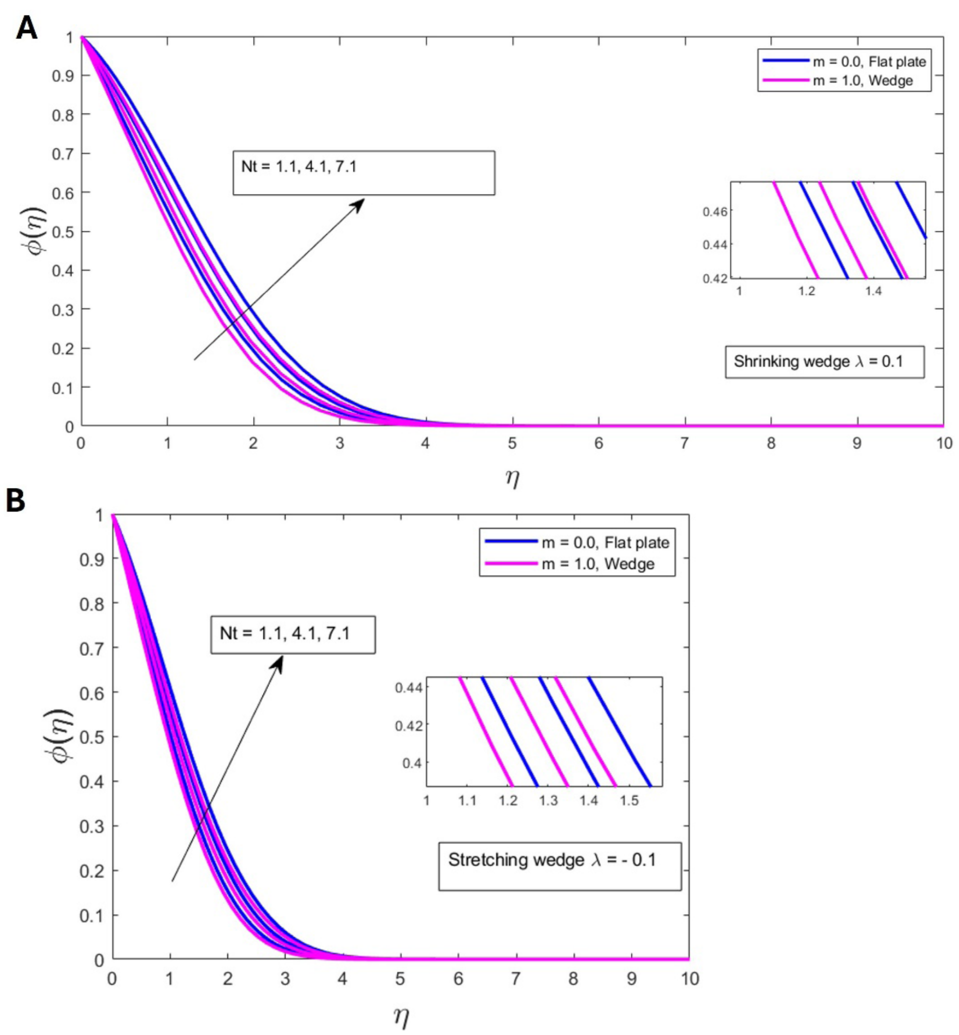

Figure 9. Nanoparticle volume concentration profiles ϕ for different values of Nt on (A) shrinking wedge and (B) stretching wedge. Parameters: $\lambda_T = 0.1; \lambda_C = 0.1; Pr = 7.0; Sc = 1.1; W = 7.1; Q = 6.1; Rd = 10.1; Nb = 10.0; \gamma = \dfrac{\pi}{6}; M = 5.0.$

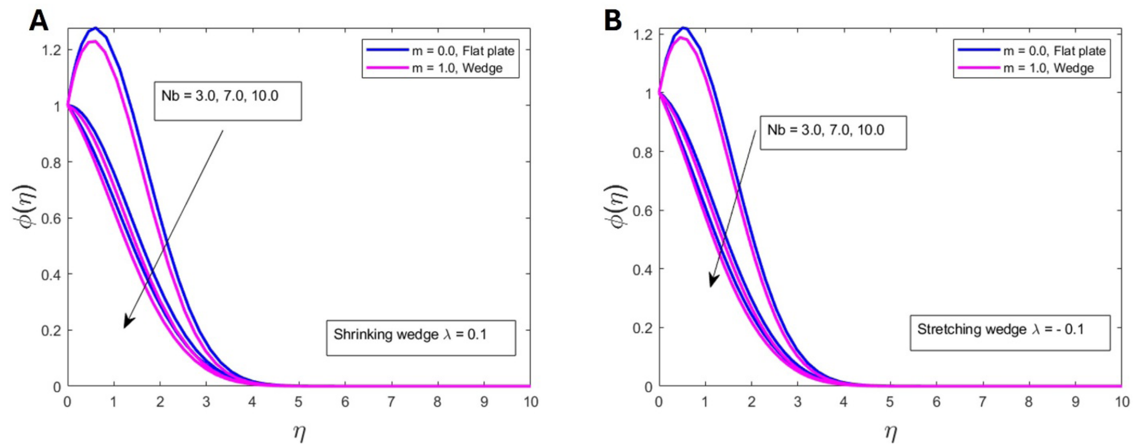

Figure 10. Nanoparticle volume concentration profiles ϕ for different values of Nb on (A) shrinking wedge and (B) stretching wedge. Parameters: $\lambda_T = 0.1; \lambda_C = 0.1; Pr = 7.0; Sc = 1.1; W = 7.1; Q = 6.1; Rd = 10.1; Nt = 7.1; \gamma = \dfrac{\pi}{6}; M = 5.0.$

Table 7. Skin friction, heat transfer rate, and nanoparticle mass transfer rate for different values of M along the stretching wedge ($\lambda = -0.1$)

M	Flat plate $m = 0.0$			Wedge $m = 1.0$		
	$f''(0)$	$-\theta'(0)$	$-\phi'(0)$	$f''(0)$	$-\theta'(0)$	$-\phi'(0)$
3.0	0.5800	0.6911	0.2570	0.8167	0.6653	0.3162
7.0	0.8226	0.6648	0.3174	1.0026	0.6507	0.3510
10.0	0.9646	0.6534	0.3445	1.1218	0.6431	0.3697

Parameters: $\lambda_T = 0.1; \lambda_C = 0.1; Pr = 7.0; Sc = 1.1; W = 7.1; Rd = 10.1; Nb = 10.0; \gamma = \dfrac{\pi}{6}; Nt = 7.1;$ at $\gamma = \dfrac{\pi}{6}$.

Table 8. Skin friction, heat transfer rate, and nanoparticle mass transfer rate for different values of M along the shrinking wedge ($\lambda = 0.1$)

M	Flat plate $m = 0.0$			Wedge $m = 1.0$		
	$f''(0)$	$-\theta'(0)$	$-\phi'(0)$	$f''(0)$	$-\theta'(0)$	$-\phi'(0)$
3.0	0.8990	0.7365	0.1551	1.2803	0.6988	0.2360
7.0	1.2897	0.6980	0.2376	1.5784	0.6786	0.2815
10.0	1.5174	0.6823	0.2731	1.7690	0.6683	0.3055

Parameters: $\lambda_T = 0.1; \lambda_C = 0.1; Pr = 7.0; Sc = 1.1; W = 7.1; Rd = 10.1; Nb = 10.0; \gamma = \dfrac{\pi}{6}; Nt = 7.1;$ at $\gamma = \dfrac{\pi}{6}$.

6. Conclusion

The current investigation is concentrated on the MHD effects on Williamson nanofluid flow along stretching and shrinking wedges. Radiation and inclined magnetic field influences, along with heat generation effects, are considered. The model is solved, and the outcomes of the parameters on the physical properties are summarized below:

(i) Increasing the Williamson fluid parameter produces a decreasing trend in the velocity profile for both shrinking and stretching wedges along the flat plate and wedge, because it generates viscosity that retards fluid motion.

(ii) A decreasing velocity field is observed with increasing magnitudes of the heat generation parameter, since momentum diffusivity increases, weakening the velocity gradient.

(iii) The heat generation parameter has a maximizing effect on the temperature profile in all cases, as the thermal boundary layer becomes thinner, leading to higher temperatures for both shrinking and stretching wedges.

(iv) The temperature profile increases with higher values of the solar radiation parameter, since its inclusion enhances the fluid temperature in the flow domain.

(v) Increasing values of the thermophoresis parameter and Brownian motion parameter raise the temperature profile.

(vi) Graphs show an increasing trend in nanoparticle volume fraction under higher values of the thermophoresis parameter for both wedge cases and the flat plate.

(vii) All results are obtained at an inclined magnetic field angle $\gamma = \pi / 6$.

(viii) A grid independence test was performed, ensuring that the solutions are grid-independent.

(ix) Comparison with existing results shows strong agreement, validating the accuracy of the present solutions.

(x) All results satisfy the boundary conditions, further confirming the reliability of the solutions.

6.1. Limitations of the current study

The present study is subject to several limitations that define the scope of the analysis:

(i) The fluid flow is considered two-dimensional.

(ii) The flow is assumed to be steady-state.

(iii) A two-phase nanofluid model (Buongiorno's nanofluid model) is employed.

(iv) Constant thermophysical properties are assumed.

(v) A simple inclined magnetic field is considered.

(vi) Viscous dissipation and Joule heating effects are neglected. Boundary-layer approximation is applied to the wedge surface.

6.2. Future scope of the current study

The present investigation opens several avenues for future research:

(i) Extension to a three-dimensional, unsteady fluid flow problem.

(ii) Consideration of variable thermophysical properties.

(iii) Inclusion of a non-uniform and time depend magnetic field.

(iv) Exploration of multiphase nanofluid models.

(v) Incorporation of Joule heating and viscous dissipating effects.

(vi) Application of entropy optimization techniques.

(vii) Coupling with other non-Newtonian fluid models.

Acknowledgments

The authors extend their appreciation to the Deanship of Scientific Research at Northern Border University, Arar, KSA, for funding this research work through the project number "NBU-FFR-2026-1902-10".

Funding

The authors extend their appreciation to the Deanship of Scientific Research at Northern Border University, Arar, KSA, for funding this research work through the project number "NBU-FFR-2026-1902-10".

Conflict of interest

The authors declare they have no competing interests.

Author contributions

Conceptualization: All authors
Investigation: Amir Abbas, Maria Gulzar
Methodology: All authors
Formal analysis: All authors
Writing – original draft: Amir Abbas, Maria Gulzar, Muhammad Farman, Evren Hincal
Writing – review & editing: All authors

Availability of data

Not applicable.

AI tools statement

All authors confirm that no AI tools were used in the preparation of this manuscript.

References

1. Ramesh GK, Gireesha BJ, Gorla RSR. Study on Sakiadis and Blasius flows of Williamson fluid with convective boundary condition. *Nonlinear Eng.* 2015;4(4):215-221.
   https://doi.org/10.1515/nleng-2015-0020
2. Priyadharshini P, Karpagam V, Gayathri P. Numerical and ANN optimization analysis for Williamson fluid flow across a porous surface. *Neural Comput Appl.* 2026;38(9).
   https://doi.org/10.1007/s00521-026-12073-4
3. Asjad MI, Zahid M, Inc M, Baleanu D, Almohsen B. Impact of activation energy and MHD on Williamson fluid flow in the presence of bioconvection. *Alex Eng J.* 2022;61(11):8715-8727.
   https://doi.org/10.1016/j.aej.2022.02.013
4. Rashid M, Ansar K, Nadeem S. Effects of induced magnetic field for peristaltic flow of Williamson fluid in a curved channel. *Phys A Stat Mech Appl.* 2020;553:123979.
   https://doi.org/10.1016/j.physa.2019.123979
5. Abbas A, Jeelani MB, Alnahdi AS, Ilyas A. MHD Williamson nanofluid flow and heat transfer past a non-linear stretching sheet implanted in a porous medium: Effects of heat generation and viscous dissipation. *Processes.* 2022;10(6):1221.
   https://doi.org/10.3390/pr10061221
6. Hussain SM. Dynamics of radiative Williamson hybrid nanofluid with entropy generation: Significance in solar aircraft. *Sci Rep.* 2022;12(1).
   https://doi.org/10.1038/s41598-022-13086-4
7. Raza J, Mebarek-Oudina F, Mahanthesh B. Magnetohydrodynamic flow of nano Williamson fluid generated by stretching plate with multiple slips. *Multidiscip Model Mater Struct.* 2019;15(5):871-894.
   https://doi.org/10.1108/MMMS-11-2018-0183
8. Hashim, Hamid A, Khan M, Khan U. Thermal radiation effects on Williamson fluid flow due to an expanding/contracting cylinder with nanomaterials: Dual solutions. *Phys Lett A.* 2018;382(30):1982-1991.
   https://doi.org/10.1016/j.physleta.2018.04.057
9. Zehra I, Yousaf MM, Nadeem S. Numerical solutions of Williamson fluid with pressure dependent viscosity. *Results Phys.* 2015;5:20-25.
   https://doi.org/10.1016/j.rinp.2014.12.002
10. Hayat T, Bibi S, Rafiq M, Alsaedi A, Abbasi FM. Effect of an inclined magnetic field on peristaltic flow of Williamson fluid in an inclined channel with convective conditions. *J Magn Magn Mater.* 2016;401:733-745.
    https://doi.org/10.1016/j.jmmm.2015.10.107
11. Ishak A, Nazar R, Pop I. Falkner-Skan equation for flow past a moving wedge with suction or injection. *J Appl Math Comput.* 2007;25(1-2):67-83.
    https://doi.org/10.1007/BF02832339
12. Maaitah H, Olimat AN, Quran O, Duwairi HM. Viscous dissipation analysis of Williamson fluid over a horizontal saturated porous plate at constant wall temperature. *Int J Thermofluids.* 2023;19:100361.
    https://doi.org/10.1016/j.ijft.2023.100361
13. Rashad AM, Nafe MA, Eisa DA. Heat variation on MHD Williamson hybrid nanofluid flow with convective boundary condition and Ohmic heating in a porous material. *Sci Rep.* 2023;13(1).
    https://doi.org/10.1038/s41598-023-33043-z
14. Salahuddin T, Khan M, Saeed T, Ibrahim M, Chu YM. Induced MHD impact on exponentially varying viscosity of Williamson fluid flow with variable conductivity and diffusivity. *Case Stud Therm Eng.* 2021;25:100895.
    https://doi.org/10.1016/j.csite.2021.100895
15. Mishra P, Kumar D, Dharmendar Reddy Y, Shankar Goud B. Numerical investigation of MHD flow of Williamson nanofluid with variable viscosity past a wedge within porous media: A non-Darcy model approach. *Heat Transfer.* 2022;51(7):6071-6086.
    https://doi.org/10.1002/htj.22580
16. Florence AD. Temperature-dependent variable viscosity and thermal conductivity effects on non-Newtonian fluids flow in a porous medium. *World*

J Eng. 2022;20(3):445-457.

https://doi.org/10.1108/WJE-03-2021-0130

17. Salahuddin T, Fatima G, Awais M, Khan M. Numerical study of the heat and mass transport along with variable viscosity of magnetohydrodynamic Williamson fluid by considering the Soret and Dufour effects: Using Milne's method. *Int J Model Simul.* 2025.

https://doi.org/10.1080/02286203.2025.2518588

18. Khan WA, Pop I. Boundary layer flow past a wedge moving in a nanofluid. *Math Probl Eng.* 2013;2013:1-7.

https://doi.org/10.1155/2013/637285

19. Mahendran MS, Wong LS, Antony Dhanapal ACT, Djearamane S. The effect of titanium dioxide nanoparticles on *Haematococcus pluvialis* biomass concentration. *J Exp Biol Agric Sci.* 2023;11(2):416-422.

https://doi.org/10.18006/2023.11(2).416.422

20. Berrehal H, Dinarvand S, Khan I. Mass-based hybrid nanofluid model for entropy generation analysis of flow upon a convectively-warmed moving wedge. *Chin J Phys.* 2022;77:2603-2616.

https://doi.org/10.1016/j.cjph.2022.04.017

21. Sajid T, Al Mesfer MK, Jamshed W, *et al.* Endo/exothermic chemical processes influences of tri-hybridity nanofluids flowing over wedge with convective boundary constraints and activation energy. *Results Phys.* 2023;51:106676.

https://doi.org/10.1016/j.rinp.2023.106676

22. Mahanthesh B, Shehzad SA, Ambreen T, Khan SU. Significance of Joule heating and viscous heating on heat transport of MoS_2–Ag hybrid nanofluid past an isothermal wedge. *J Therm Anal Calorim.* 2020;143(2):1221-1229.

https://doi.org/10.1007/s10973-020-09578-y

23. Dawar A, Shah Z, Tassaddiq A, Kumam P, Islam S, Khan W. A convective flow of Williamson nanofluid through cone and wedge with non-isothermal and non-isosolutal conditions: A revised Buongiorno model. *Case Stud Therm Eng.* 2021;24:100869.

https://doi.org/10.1016/j.csite.2021.100869

24. Nasir M, Ali AB, Anwar T, *et al.* Impact of liquid hydrogen in stagnation-point flow of hydromagnetic Williamson nanomaterial configured by a stretched vertical wedge featuring nonlinear chemical reaction. *Case Stud Therm Eng.* 2025;75:107122.

https://doi.org/10.1016/j.csite.2025.107122

25. Patil VS, Humane PP, Patil AB. MHD Williamson nanofluid flow past a permeable stretching sheet with thermal radiation and chemical reaction. *Int J Model Simul.* 2022;43(3):185-199.

https://doi.org/10.1080/02286203.2022.2062166

26. Hussain M, Lubna A, Ashraf M, Anwar MS, Ranjha QA, Ali A. Ohmically dissipated MHD mixed convective flow of Williamson fluid over a penetrable stretching convective wedge with thermal radiations. *Numer Heat Transfer B Fundam.* 2023;85(8):1026-1040.

https://doi.org/10.1080/10407790.2023.2261623

27. Abbas A, Khandelwal R, Ahmad H, *et al.* Magnetohydrodynamic bioconvective flow of Williamson nanofluid over a moving inclined plate embedded in a porous medium. *Mathematics.* 2023;11(4):1043.

https://doi.org/10.3390/math11041043

28. Usman, Lin P, Ghaffari A. Heat and mass transfer in a steady flow of Sutterby nanofluid over the surface of a stretching wedge. *Phys Scr.* 2021;96(6):065003.

https://doi.org/10.1088/1402-4896/abecf7

29. Oderinu RA, Oyeyinka TA, Alao S, Ayanbukola FJ, Sanusi BA. Mixed convection and permeability effects on magnetohydrodynamic Williamson fluid flow over an inclined stretchy surface with radiation influence: Analytical investigation. *Eng Rep.* 2025;7(4).

https://doi.org/10.1002/eng2.70078

30. Alao S, Abdulkareem FA, Ogunmola OJ, Oderinu RA. Theoretical investigation of heat and mass transfer in unsteady magnetohydrodynamic Williamson nanofluid flow past a permeable stretching surface with viscous dissipation effect. *Therm Adv.* 2026;6:100101.

https://doi.org/10.1016/j.thradv.2026.100101

31. Sankari MS, Rao ME, Shams ZE, *et al.* Williamson MHD nanofluid flow via a porous exponentially stretching sheet with bioconvective fluxes. *Case Stud Therm Eng.* 2024;59:104453.

https://doi.org/10.1016/j.csite.2024.104453

32. Obalalu AM, Salawu SO, Olayemi OA, Ajala OA, Issa K. Analysis of hydromagnetic Williamson fluid flow over an inclined stretching sheet with Hall current using Galerkin Weighted Residual Method. *Comput Math Appl.* 2023;146:22-32.

https://doi.org/10.1016/j.camwa.2023.06.021

33. Sankari S, Rao ME, Elsiddieg AM, *et al.* Analytical solution of MHD bioconvection Williamson nanofluid flow over an exponentially stretching sheet with the impact of viscous dissipation and gyrotactic microorganism. *PLoS ONE.* 2025;20(3):e0306358.

https://doi.org/10.1371/journal.pone.0306358

34. Priyadharshini P, Karpagam V, Shah NA, Alshehri MH. Bio-convection effects of MHD Williamson fluid flow over a symmetrically stretching sheet: Machine learning. *Symmetry.* 2023;15(9):1684.

https://doi.org/10.3390/sym15091684

35. Naz S, Hayat T, Momani S. Dufour and Soret features in entropy optimized Williamson fluid with nonlinear thermal radiation: Modified Darcy law analysis. *Results Eng.* 2025;25:104293.

https://doi.org/10.1016/j.rineng.2025.104293

36. Swalmeh MZ, Alwawi FA, Kausar MS, *et al.* Numerical simulation on energy transfer enhancement of a Williamson ferrofluid subjected to thermal radiation and a magnetic field using hybrid ultrafine particles. *Sci Rep.* 2023;13(1).

https://doi.org/10.1038/s41598-023-29707-5

37. Zafar SS, Zaib A, Lone SA, Mahnashi AM, Hamali W, Saeed A. Numerical analysis of Williamson nanofluid over lubricated surface due to microorganism with thermal radiation. *J Therm Anal Calorim.* 2025;150(4):2319-2334.

https://doi.org/10.1007/s10973-023-12874-y

38. Akbar S, Sohail M, Abbas ST, Badi N. Optimal homotopic strategy for thermal and mass transport in Williamson model flow PDEs under heat generation/absorption and Joule heating. *Adv Mech Eng.* 2024;16(11):16878132241294262.

https://doi.org/10.1177/16878132241294262

39. Znaidia S, Rehman S, Drissi N, Asiri F, Nasr S. Mixed convection flow and heat transfer of Williamson drilling nanofluid over a stretching cylinder using Brinkman-Maxwell-Garnett model and temperature-dependent features. *J Nonlinear Math Phys.* 2025;32(1).

https://doi.org/10.1007/s44198-025-00292-7

40. Zafar SS, Zaib A, Lone SA, Mahnashi AM, Hamali W, Saeed A. Radiative heat in a Williamson fluid flow through a lubricated surface containing swimming microorganism. *J Therm Anal Calorim.* 2025;150(4):2633-2650.

https://doi.org/10.1007/s10973-023-12861-3

Dr. Amir Abbas *received his Ph.D. in Applied Mathematics (Computational Fluid Dynamics and Heat Transfer) from the University of Sargodha in 2021. He is an Assistant Professor at Baba Guru Nanak University, Pakistan, and is currently engaged in postdoctoral research at Near East University, Türkiye. His research focuses on computational fluid dynamics and heat transfer. He has published over 60 research papers and has an H-index of 31.*

Dr. Akhlaqur Rahman *received his Ph.D. in Electrical and Electronic Engineering from Swinburne University of Technology in 2019. He is currently a Senior Lecturer and Course Coordinator at the Engineering Institute of Technology. His research interests include cloud networked robotics, machine learning, industrial automation, network optimization, smart manufacturing, and the Internet of Things (IoT).*

Ms. Maria Gulzar *received her BSc in Mathematics from Government College for Women, Jhang, and her MSc in Applied Mathematics from Government College University, Faisalabad, Pakistan. She is currently pursuing an MS degree in Applied Mathematics. Her research interests include computational fluid dynamics and heat transfer, and she has several years of teaching experience.*

Dr. Muhammad Farman *received his Ph.D. in Mathematics from the University of Lahore in 2019 and completed postdoctoral fellowships at several international universities. He is currently an Associate Professor at Near East University. His research interests include mathematical biology, control theory, numerical analysis, and fractional calculus. He has published over 300 research papers and has an H-index of 37.*

Prof. Dr. Mohamed Ahmed Hafez *is a civil engineering researcher and academic with over 30 years of research and consultancy experience. His expertise includes coastal engineering, erosion prevention, ground improvement, slope stability, dam safety, and reservoir sedimentation. He has authored five books, contributed to over 170 publications, supervised more than 30 postgraduate students, and received several national and international awards.*

Dr. Evren Hinçal *is a Professor of Mathematics at Near East University. He received his undergraduate degree from Hacettepe University and his master's degree from Imperial College London. His research background includes applied mathematics and cancer epidemiology. He has authored numerous international publications and has participated in many international conferences.*

Dr. Sk. Arefin Shezan *is an Assistant Professor of Electrical Engineering at Northern Border University, Saudi Arabia, with extensive international academic experience. He received his Ph.D. in Electrical and Electronic Engineering from RMIT University, Australia, in 2021. His research interests include renewable energy integration, microgrids, power systems, solar and wind energy, optimization, control systems, and energy economics.*

Dr. Naveed Ahmad *is an Assistant Professor in the Department of Chemical and Materials Engineering at*

Northern Border University, Saudi Arabia. He holds a Ph.D. from the University of Naples Federico II. His research expertise includes polymer rheology, wastewater treatment, energy engineering, and advanced materials for sustainable energy and environmental applications.